

Article

Influence of Heat Treatment on Microstructure and Mechanical Properties of Laser Cladding Coatings

Chen Yang ¹, Wenjing Chen ^{1,*}, Bo Tan ¹, Qingsong Luo ¹, Tao Cao ¹ and Zhenlin Zhang ²

¹ School of Materials Science and Engineering, Xihua University, Chengdu 610039, China; ncyangchen23@163.com (C.Y.); tb2976018533@163.com (B.T.); s1753776@163.com (Q.L.); 18583304237@163.com (T.C.)

² School of Material Science and Engineering, Southwest Jiaotong University, Chengdu 610031, China; zzl21@swjtu.edu.cn

* Correspondence: 0720080005@xhu.edu.cn

Abstract: This study investigates the influence of various heat treatment processes on the microstructure and properties of laser cladding Fe314 coatings. The microstructure, phases, and impact fracture morphology of the cladding layer were observed using X-ray diffraction and scanning electron microscopy, among other methods. The hardness and impact performance of the cladding layer were also tested. The results indicated that there was compositional segregation and non-equilibrium microstructure in the untreated cladding layer, with an average microhardness of 368.67 HV and an impact toughness of 27 J, exhibiting quasi-cleavage fracture. The stress-relief annealing treatment resulted in a uniform distribution of M23C6 carbides inside the cladding layer. The pinning effect generated by M23C6 reduced the microhardness by 16.26% and increased the impact toughness to 54 J. The impact fracture surface exhibited ductile fracture. After secondary normalizing and annealing, the microstructure of the cladding layer transformed into a fine single-phase austenite structure, and fine M7C3 carbides precipitated at the grain boundaries. Under the effects of fine grain strengthening and dispersion strengthening, the microhardness of the cladding layer decreased by 38.14%, and the average impact absorbed energy of the specimen was 64 J, showing complete ductile fracture.

Keywords: laser cladding; microstructure; heat treatment process; mechanical properties



Citation: Yang, C.; Chen, W.; Tan, B.; Luo, Q.; Cao, T.; Zhang, Z. Influence of Heat Treatment on Microstructure and Mechanical Properties of Laser Cladding Coatings. *Coatings* **2024**, *14*, 1251. <https://doi.org/10.3390/coatings14101251>

Academic Editor: Andrew J. Pinkerton

Received: 28 August 2024

Revised: 23 September 2024

Accepted: 24 September 2024

Published: 1 October 2024



Copyright: © 2024 by the authors. Licensee MDPI, Basel, Switzerland. This article is an open access article distributed under the terms and conditions of the Creative Commons Attribution (CC BY) license (<https://creativecommons.org/licenses/by/4.0/>).

1. Introduction

EA4T steel is the main material used for manufacturing locomotive axles due to its excellent overall mechanical properties [1]. However, when locomotives operate on high-speed tracks, the axle surface may encounter external damage caused by sharp and hard objects [2]. Therefore, exploring an environmentally friendly axle remanufacturing and repair technology not only reduces the waste of resources, but also reduces the maintenance cost of trains. Laser cladding is a rapid heating and cooling process that results in the formation of a fine grain structure with high bond strength in the cladding layer. However, the rapid solidification during cladding can lead to elemental segregation, resulting in severe lattice distortions in the cladding, which can degrade the properties of the cladding [3]. How to control the quality of the clad layer in laser cladding remanufacturing is a technical challenge in axle repair and remanufacturing, and is also one of the current research focuses [4].

Currently, common methods to enhance the cladding quality include the optimization of laser process parameters [5], the addition of alloying elements [6], the application of external auxiliary fields, and post-heat treatment [7]. Chen et al. [8] utilized laser cladding technology to prepare a Fe314 clad layer on EA4T steel. By optimizing the process parameters, they obtained a set of specimens with the best match of strength and toughness. However, due to the inhomogeneous distribution of solute atoms during laser cladding,

the microhardness value of the cladding layer is relatively high. In order to enhance the performance of the fused cladding layer, Chen et al. optimized it by introducing rare earth elements in the cladding process. Rare earth elements have a role to play in grain refinement, resulting in improved toughness in all regions of the clad layer. Building upon this, Chen et al. [9] employed ultrasonic vibration-assisted laser cladding for surface repair of EA4T steel. This approach transformed the originally directionally solidified dendritic structure into a fractured dendritic and granular structure, providing a more uniform distribution of microstructure within the cladding.

All these methods can to some extent modify the microstructure and mechanical properties of fused cladding layers. However, compared to these optimization approaches, heat treatment has multiple beneficial effects on laser-clad layers. Firstly, it can eliminate residual stress, preventing cracking and delamination of the clad layer, thus enhancing safety and reliability [10]. Secondly, heat treatment can adjust the phase constitution and distribution of the fusion cladding to make the microstructure more homogeneous and stable, and enhance the resistance to crack extension [11]. Additionally, heat treatment can refine the grain size, reduce hardness, significantly improve toughness, and extend the service life [12]. Therefore, heat treatment process studies are essential to improve the quality and overall performance of the remanufactured EA4T axle cladding layers. The temperature and cooling rate during heat treatment can have a significant impact on the microstructure of the fused cladding, whereby researchers have studied and determined the correlation of microstructure with mechanical properties [13,14]. Liu et al. [15] applied a 2.0 wt.% CeO₂ Ni₆₀ self-lubricating wear-resistant composite layer on the face of 35Cr-MoV steel by laser. The heat-treated composite layer exhibited a microstructure mainly composed of equiaxed grains, with refined grain size and a uniform structure. The heat treatment promoted the refinement and nucleation of CeO₂, further refining the microstructure. Ge et al. [16] annealed lightweight steel with austenite ferrite structure at different temperatures, resulting in an increase in the austenite phase and regular distribution of the ferrite phase along grain boundaries, as well as grain refinement. This greatly reduced the residual stress level of the steel and improved its toughness. Liu et al. [17] conducted multiple normalizing treatments on 9Cr-2.3W-3.0Co martensitic steel and found that the toughness of the material increased from 182.8 J to 369.7 J after secondary normalizing. The particle size of M23C7 in the matrix decreases with the increase in normalizing times and is uniformly distributed in the matrix.

Moreover, in multi-stage annealing heat treatment, the various stages of the process interact with one another [18,19]. The changes in the microstructure of alloys under heat treatment have been extensively studied by many researchers, and have found that the transformation of metastable phases to stable phases, as well as morphological and dimensional changes in the composition of the second phase in the fused cladding, can affect both the strength and toughness of the fused cladding [19]. Shi et al. [20] prepared a 34CrNiMo6 cladding layer by laser cladding technique. The effects on microstructure and mechanical properties of alloys with different tempering treatments were investigated. It was observed that as the tempering temperature increased, the bar and plate carbides gradually transformed into stable coarse-grained carbides, and thermal treatment removed the microstructural inhomogeneity in samples, thus improving the toughness of the fused cladding. Zhao et al. [21] prepared an iron-based fusion cladding on 3Cr13 stainless steel using laser cladding technology and controlled the microstructure of the coating by solution aging. The carbides in the fused cladding were transformed from blocky, dendritic, and consecutive intergranular morphology to spherical, discontinuous, and short rod-like morphology, which greatly enhanced the uniformity of the microstructure.

For enhancing the comprehensive performance of laser composite Fe314 layers, this study investigates the microstructural evolution of the Fe314 laser-clad layer and the precipitation phases under different heat treatment processes, namely stress-relief annealing and secondary austenitizing with tempering. Furthermore, the effect of these

microstructural changes on the mechanical properties of cladding layers was investigated and analyzed.

2. Materials and Methods

2.1. Experimental Equipment and Materials

The matrix material used for the test in this paper is EA4T axle steel developed by Siemens, Germany, which belongs to low carbon and low alloy steel, and its main chemical composition is shown in Table 1. The powder used in the experiment were spherical Fe314 powders (provided by BGRIMM Advanced Materials Science & Technology Co., Ltd., Beijing, China) with particle diameters of 90–120 μm (as shown in Figure 1), the powder fluidity is 30.78 g/s, the bulk density is 4.537 g/cm³, the thermal expansion coefficient of Fe314 is similar to that of EA4T steel, and the main chemical composition is shown in Table 2.

Table 1. Main chemical composition of EA4T steel (wt. %).

C	Cr	Si	Ni	Mn	Mo	Cu	S	P	Fe
0.24	1.04	0.34	0.26	0.74	0.25	0.15	0.002	0.008	Bal.

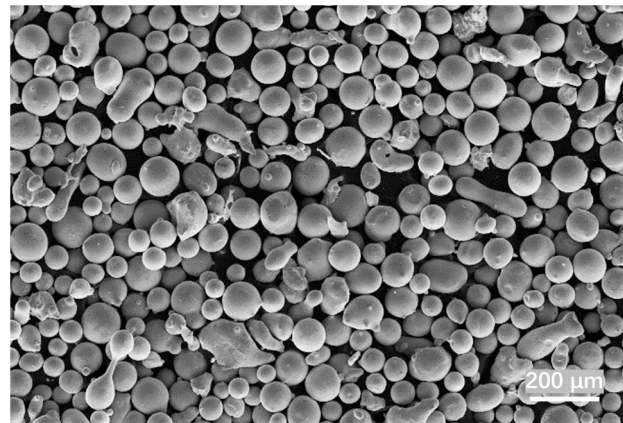


Figure 1. Micro-morphology of the Fe314 alloy powder.

Table 2. Composition of Fe314 alloy powder (wt. %).

C	Si	Cr	Ni	B	Fe
0.1	0.12	17.5	10.5	0.65	Bal.

A 6 kW fiber laser (YLS-6000 IPG, IPG Photonics, Marlborough, MA, USA) with a spot diameter of 3 mm and a wavelength of 1070 nm was used in the experiments. The powder-feeding system of HUIRUI-O4T adopts a double-cylinder powder feeder (Nanjing, China), and the powder-feeding speed is mainly regulated by adjusting the rotational speed of the powder feeder disc. The powder material consists of spherical Fe314 particles and is transported through the powder-feeding nozzle using high-purity argon up to 99.999%. The cladding layer thickness is maintained at 1.2–1.5 mm (this is the result after strictly controlling the experimental variables), while laser power is 2.2 KW, the powder-feeding speed is 2.5 r/min, the scanning speed is 4.67 mm/s, and the powder-feeding gas flow rate and protective gas flow rate are 22 L/min and 5 L/min, respectively [22].

2.2. Experimental Methods

Laser cladding of two-dimensional planar surfaces can be achieved by a four-axis linked CNC platform, and the laser scanning direction can be realized along the X and Y axes according to the CNC programming system. Process parameters like overlap rate

and scanning speed can be set by the CNC programming system (UG NX 2000) in the computer, and the laser-fused specimens were heat treated in a vacuum furnace (MXQ1700-40, working vacuum degree ≥ -0.05 MPa, Micro-X, Shanghai, China) [23]. Rapid changes in temperature during the cladding process can lead to significant internal stresses within the clad sample. To alleviate the residual stresses generated in the cladding process and to improve cladding properties, the laser-cladded samples were subjected to two types of heat treatment: annealing treatment and secondary normalizing + annealing, respectively. At the same time, untreated laser-cladded samples are utilized as control specimens. The specific heat treatment processes are detailed in Table 3.

Table 3. Heat treatment process parameters.

Process	Stage	Temp (°C)	Soaking (h)	Rate (°C/min)
Annealing	Step 1	550	2	10
	Step 1	1150	1	3
Secondary normalizing + annealing	Step 2	980	1	3
	Step 3	650	2	10

After grinding and polishing, the overlay of the specimen was etched with a FeCl_3 solution ($\text{FeCl}_3:\text{HNO}_3:\text{HCl}:\text{C}_2\text{H}_5\text{OH} = 2:3.5:1:30$) to prepare a metallographic specimen. The microstructure, phase analysis, and impact fracture morphology of the alloy were observed using an X-ray diffractometer (D8 advance, Bruker, Billerica, MA, USA), and a scanning electron microscope (S-3400N, Hitachi, Tokyo, Japan). The microhardness of the specimen is tested from the surface of the cladding to the substrate using a JMHVS-1000AT hardness tester (DONGHUA, Taizhou, China). The test distance was 100 μm , the hardness test load was 1.96 N, and the load holding time was 20 s. The test process was conducted in accordance with GB/T4340.1-2009 [24]. The impact specimens were processed into standard U-notch specimens of 55 mm \times 10 mm \times 10 mm based on the Chinese national standard GB/T 229-2007 [25], and a JB-300B impact tester (JINANCHENXIN, Jinan, China) for room temperature impact testing. The dimensions of the specimen are shown in Figure 2.

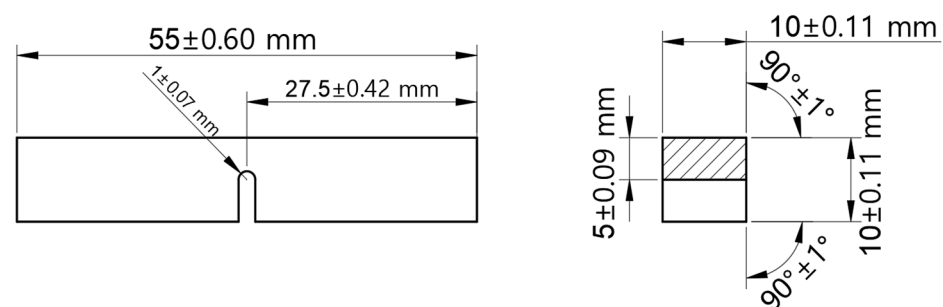


Figure 2. Schematic diagram of the U-notched Charpy impact specimens.

3. Results and Discussion

3.1. Microstructural Analysis

Figure 3 shows the organization of the fused cladding without heat treatment, annealed, and after secondary normalization plus annealing, respectively. The optimum process parameters were determined through preliminary tests. As shown in Figure 3a, the surface of the fused cladding layer was well formed without defects such as cracks and porosity. As shown in Figure 3b, the microstructural morphology of unheat-treated fused coatings consists mainly of dendritic crystals. Laser cladding technology is characterized by rapid cooling and heating, the solidification process deviates from the equilibrium state, and the diffusion process is too late to fully carry out, resulting in the cladding layer dendritic segregation, which makes the cladding layer plasticity and toughness very

poor, and therefore the repaired axle often do not meet the toughness requirements for the conditions of use. Significant changes in the organization of the fused cladding after annealing at 550 °C for 2 h, reduction in reticulation, and the dendritic crystal chains were interrupted to form rod-like crystals, but there are still obvious dendritic structures in the cladding layer after stress-relief annealing treatment, show that stress-relief annealing will not alter the phase composition inside the cladding layer (as in Figure 3c). After two normalizations plus annealing, the grains in the fused coatings become uniformly fine and tightly structured. The fused cladding consists mainly of a dark matrix and a short grey-white rod-like precipitated phase. Pits formed by the shedding of fine grains can be identified at the surface of the cladding (Figure 3d) [26].

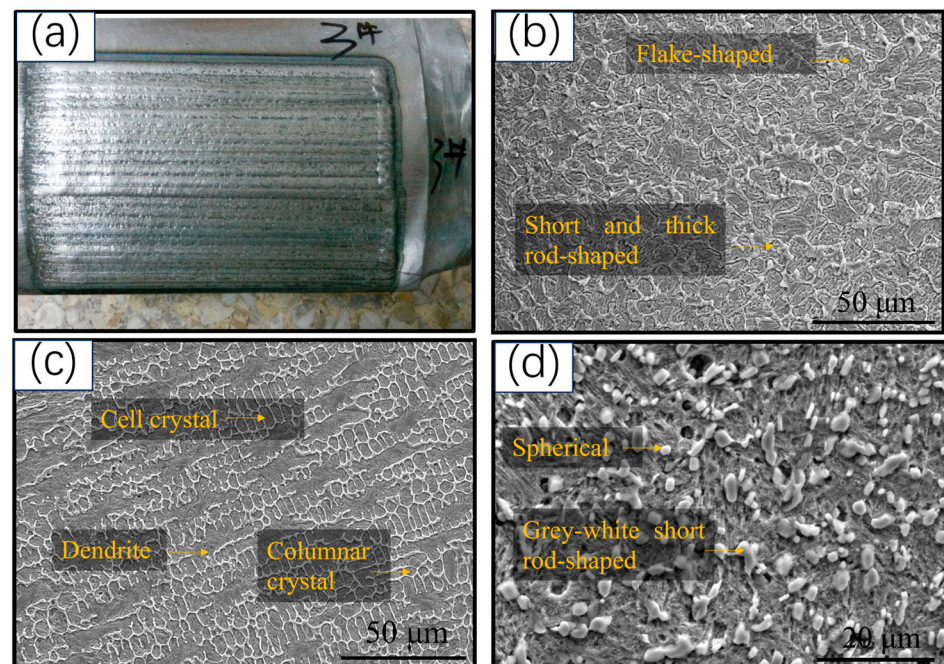


Figure 3. Macroscopic schematic and SEM images: (a) macroscopic schematic; (b) unannealed; (c) annealed; (d) normalized + annealed.

By comparison, it can be found that due to the instantaneous completion of the laser cladding process and the rapid temperature changes inside the melt pool, the alloy elements in the material cannot diffuse in time, resulting in non-free diffusion crystallization. Unheated specimens exhibit microstructures that show segregation. After annealing at 550 °C for 2 h, due to the heat treatment temperature not reaching the phase transition temperature, no new phases were generated inside the melt pool. However, the microstructure produced by annealing was homogenized, which improved the segregation of the microstructure and reduced the residual stress of the microstructure. After secondary normalizing and annealing treatment, as the temperature reaches the austenitization temperature, the alloy elements further diffuse and dissolve, and the disappearance of dendritic crystals grown along grain boundaries, producing a large number of elliptical hard phases at the grain boundaries.

Figure 4 presents the XRD results for untreated and heat-treated samples. It can be observed from the results that, both in the untreated and annealed conditions at 550 °C for 2 h, the austenite phase is abundant in the microstructure of the cladding layer, with a uniform distribution of (Cr, Fe)₂₃C₆ carbides between the dendrites. These carbides are identified as hard phases, which can pin dislocations and hinder the deformation of the austenite. The annealing did not alter the phase in the cladding layer, but rather ensured uniform distribution of (Cr, Fe)₂₃C₆ in the microstructure, thereby eliminating residual stress within it.

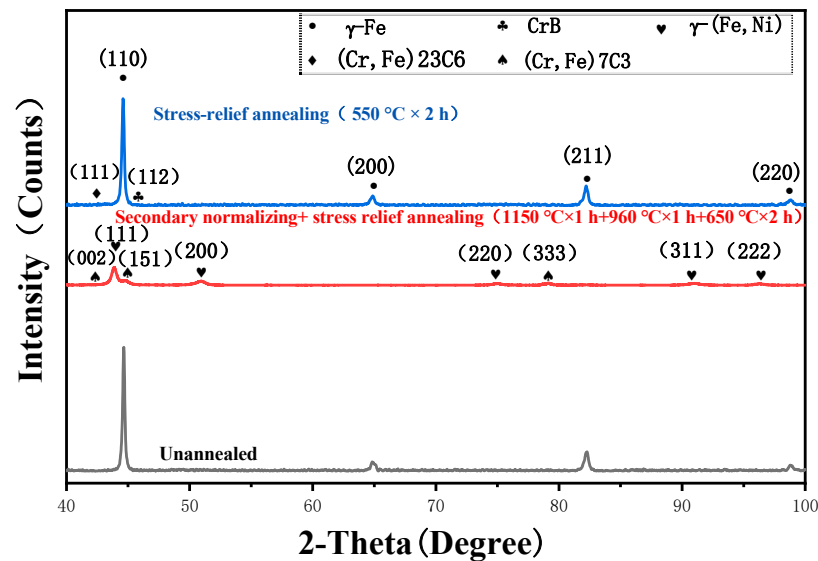


Figure 4. The XRD results of the cladding layer under different heat treatment conditions.

After secondary normalization and annealing, the main components of the cladding are the γ -(Fe, Ni) phase and (Cr, Fe)7C3 carbides. In the first stage of heat treatment, the high-temperature treatment at 1150 °C can cause all M23C6 carbides and CrB compounds in the cladding layer to remelt into austenite, and the cladding layer undergoes complete recrystallization, equivalent to a solid solution treatment. Due to the stabilizing γ phase and diffusion effect of Ni elements during the cooling process, and the effect of Cr elements to reduce the austenite region, the transformation of austenite to martensite is inhibited during cooling, thus retaining the austenitic single-phase structure [27]. After the second stage of normalization, a significant amount of fine-grained M7C3 was precipitated in the γ -phase matrix. This is due to the fact that the holding time of 980 °C results in a large number of alloying elements being supersaturated and uniformly distributed in the austenite phase of the fusion cladding so that the Cr and C elements precipitate during the subsequent heat treatment and diffuse over short distances to form M7C3. The third stage of stress-relief annealing did not produce any phase and structural changes in the cladding layer; therefore, after secondary normalizing and annealing, the fused cladding consists mainly of austenite and M7C3 carbides. Remelting and recrystallization of the organization in the fused coating layer occur because of secondary normalization. This results in a uniform distribution of Cr, Ni, and other alloying elements, and a considerable amount of fine-grained M7C3 precipitating from the γ -phase grain boundaries [28].

3.2. Mechanical Properties

3.2.1. Microhardness Test

As shown in Figure 5, the fused cladding layer undergoes different heat treatment processes and exhibits varying microhardness. The untreated cladding layer sample demonstrates a relatively gradual change in microhardness, with a maximum microhardness of 393.2 HV and an average microhardness of 368.67 HV. Following the annealing treatment at 550 °C for 2 h, the average microhardness of the fused cladding decreases to 308.73 HV, approximately 16.26% below the untreated condition. Subsequently, the fused cladding sample subjected to secondary normalization and annealing exhibits the lowest microhardness, with an average value of 228.05 HV, representing a reduction of approximately 38.14% compared to the untreated state. These hardness changes are closely related to the evolution of the microstructure, as confirmed by the microscopic examination and XRD test results. The annealing treatment does not induce phase transformation in the cladding layer, but rather alleviates the internal structure of the grains, leading to a reduction in internal stress and, consequently, a decrease in material hardness. In contrast, the secondary

normalization and annealing treatment further alters the material's phase composition and lattice structure; the normalization treatment results in the complete transformation of the existing carbide phase into a single-phase austenitic structure. During the annealing process, numerous fine M7C3 particles precipitate from the austenitic phase boundaries, leading to a significant reduction in microhardness. By comparing the microhardness of the substrate, it can be seen that the average microhardness is 308.82 HV. After annealing treatment, the microhardness of the substrate is reduced to 207.48 HV on average, which is about 32.82% lower than that of the unheat-treated state. After the second normalizing + annealing treatment, the microhardness of the fused cladding samples was the lowest, with an average microhardness of 175.63 HV, which indicates that the heat treatment also has an obvious improvement effect on the microhardness of the matrix.

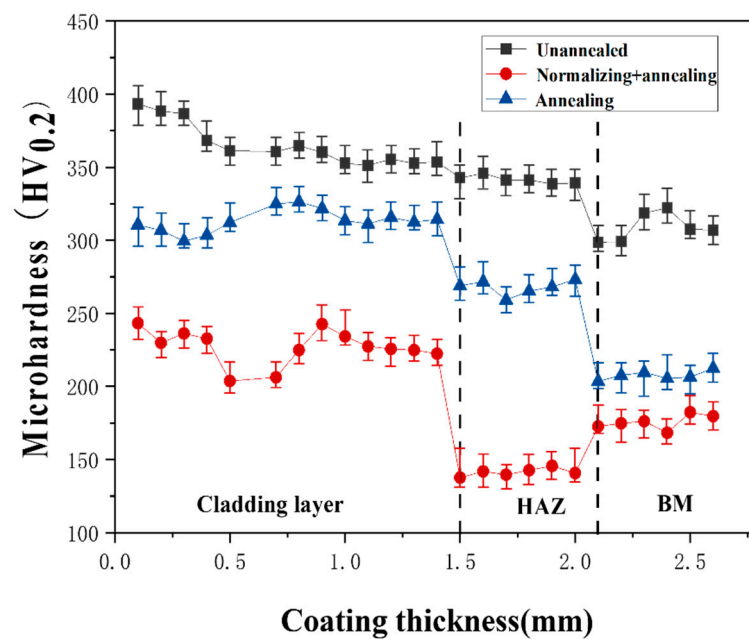


Figure 5. Microhardness curves of specimens in different states.

3.2.2. Impact Performance Testing

The Charpy impact absorption energy is a method for evaluating the toughness of materials, representing the ability of a material to absorb impact energy. When the sample sizes are equal, a greater impact absorption energy indicates a stronger resistance of the material to external impacts. According to Figure 6, the average Charpy impact absorbed energy of the untreated specimen is 27 J. This value increases to 54 J after annealing at 500 °C for 2 h. Furthermore, the cladding layer sample subjected to secondary normalization and annealing exhibits the highest impact toughness, reaching 64 J, which is 2.37 times that of the untreated sample. This indicates that after the secondary normalization and annealing treatment, there is a significant improvement in the toughness of the cladding sample. This approach has the ability to optimize the microstructure of the fused cladding, thus improving its impact resistance. Through the double normalization treatment, recrystallization occurred in the cladding layer, leading to grain refinement. Meanwhile, a large number of fine alloy carbide M7C3 particles precipitated at the austenite grain boundaries, serving as pinning sites that noticeably inhibit the growth of austenite grains, thus enhancing the toughness of the fused cladding. Furthermore, the residual stresses in the fused cladding were alleviated through stress-relief annealing, further enhancing its impact resistance [29].

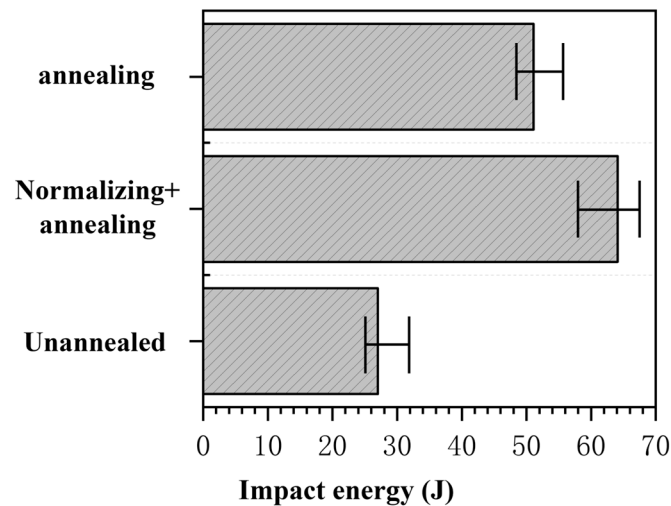


Figure 6. Impact toughness of cladding layer under different heat treatment conditions.

3.3. Impact Fracture Morphology

Figure 7 shows the impact fractures of the fused cladding under different heat treatment conditions. The fracture surface of the untreated cladding presents a smooth blocky shape with undulations and a small number of fracture planes, and tearing edges and secondary cracks can also be observed (as shown in Figure 7a). This may be due to the presence of anisotropic structures in the cladding layer. During the impact process, stress concentrates in certain areas, leading to the formation of smooth blocky shapes with undulations. These small planes may be formed due to uneven mechanical stress distribution and damage in specific areas, which is manifested as a brittle fracture on a macroscopic scale and a local quasi-cleavage fracture mechanism on a microscopic scale. Figure 7b shows the impact fracture of the coating after secondary normalizing and annealing. The impact fracture is covered by a ductile fracture zone, indicating that the cladding layer has a certain degree of toughness under impact load. In the microscopic fracture, a large number of dense pits can be seen, and the size of the holes in the pits is unevenly distributed. Overall, the impact fracture of the cladding after secondary normalizing and annealing shows the characteristics of a ductile fracture, which is quite different from the brittle fracture morphology of the untreated cladding. Figure 7c shows the microscopic morphology of the impact fracture after stress-relief annealing at 550 °C for 2 h. There are a large number of small, dense, and irregularly shaped dimples in the fracture, and the dimples are shallow, showing a complete ductile fracture.

Comparative analysis of the fused cladding with various heat treatment conditions reveals that the specimen in the secondary normalizing plus annealing has dimples of varying sizes and depths. However, in the specimens that are untreated and annealed at 550 °C for 2 h, the dimples are evenly distributed, presenting an equiaxed dimple morphology, and there are many small dimples on the large dimples. This indicates that the fused cladding in the secondary normalizing plus annealing has a more uniform structure and deformation than the untreated and 550 °C for 2 h annealed states, better relative toughness, and better performance stability. After secondary normalizing and annealing, a large amount of austenite was present in the cladding according to the microstructural analysis. During the plastic deformation process, the austenite in the cladding layer has a stronger plastic deformation ability, can consume a large amount of deformation work, and has the ability to hinder crack propagation, thus causing the phenomenon of small dimples surrounding and enclosing. Meanwhile, the granular M7C3 in the fused cladding inhibits the deformation of the austenite, indirectly improving the crack instability resistance of the cladding layer [30].

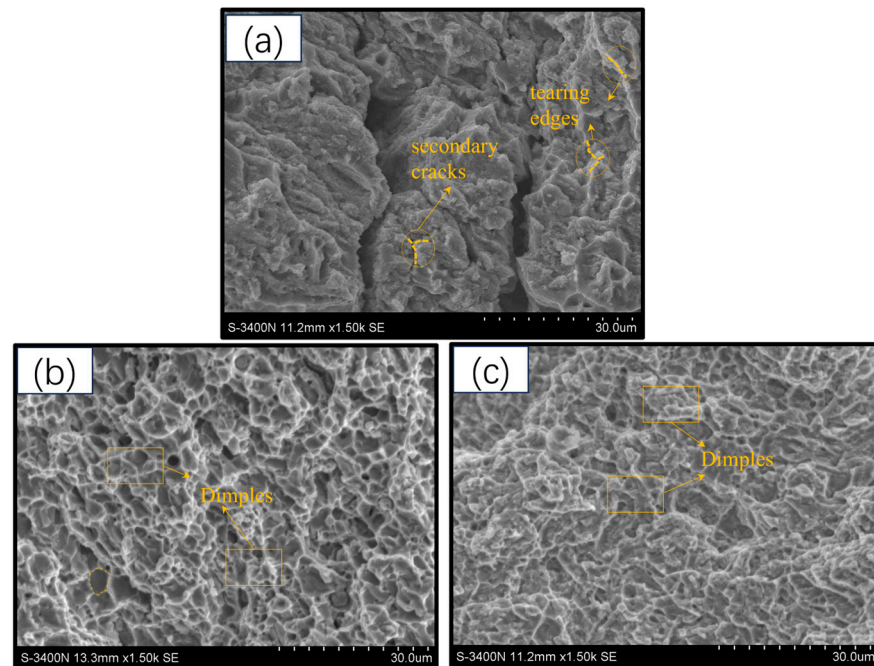


Figure 7. The impact fracture surface morphologies of the cladding layer under different heat treatments: (a) unannealed; (b) normalizing + stress-relief annealing; (c) stress-relief annealing.

4. Conclusions

This article investigates the microstructure and properties of laser cladding Fe314 alloy coatings under different heat treatment processes. The major conclusions are shown below as follows:

1. During the laser cladding process, compositional segregation and non-equilibrium microstructure exist in the fused cladding due to rapid cooling and non-diffusion crystallization, leading to higher hardness, lower toughness, and substantial residual stress. These unfavorable factors can impact the service life and reliability of the fused cladding, thus necessitating the implementation of reasonable heat treatment processes for enhancement.
2. After stress-relief annealing treatment, the M23C6 alloy carbides generated in the cladding layer were evenly distributed, which caused a pinning effect on dislocations and reduced residual stress inside the cladding layer. The average microhardness decreased by 16.26%, and the impact toughness was twice that of the untreated state. The impact fracture was distributed with a large number of small and dense ductile dimples, manifested as ductile fracture.
3. After secondary normalizing and annealing treatment, the supersaturated γ -phase and M23C6 carbides in the organization transformed into fine single-phase austenite structures, and fine M7C3 carbides precipitated at the austenite grain boundaries. Under the effects of fine grain strengthening and dispersion strengthening, the average microhardness of the sample decreased by 38.14%, and the impact toughness increased to 2.37 times that of the untreated sample. Compared with the stress-degraded sample, the distribution of toughness dimples on the impact fracture surface was more uniform and dense, showing better toughness and performance stability.

Author Contributions: Conceptualization, W.C. and C.Y.; methodology, B.T.; validation, W.C., C.Y. and T.C.; formal analysis, C.Y.; investigation, C.Y.; resources, Q.L.; data curation, W.C.; writing—original draft preparation, C.Y.; writing—review and editing, Z.Z.; supervision, W.C. and Z.Z.; project administration, B.T.; funding acquisition, W.C. All authors have read and agreed to the published version of the manuscript.

Funding: This research was supported by the National Natural Science Foundation of China, grant number 52375387.

Institutional Review Board Statement: Not applicable.

Informed Consent Statement: Not applicable.

Data Availability Statement: Data are contained within the article.

Conflicts of Interest: The authors declare no conflicts of interest.

References

- Li, J.; Yang, Y.; Chen, L.; Sun, B.; Wang, Z.; Yu, T.; Zhao, J. The effects of in-situ synthesized TiC on the performance improvement of nickel-based composite coatings for rail repair. *Ceram. Int.* **2024**, *50*, 28628–28640. [\[CrossRef\]](#)
- Jin, J.; Chen, B.; Zhang, Z.; Wu, Y.; Luo, Z.; Gou, G.; Chen, W. Effects of Mo content on the microstructure and mechanical properties of laser cladded FeCoCrNiMox ($x = 0.2, 0.5$) high-entropy alloy coatings. *Surf. Coat. Technol.* **2024**, *482*, 130697. [\[CrossRef\]](#)
- Hamilton, J.D.; Sorondo, S.; Li, B.; Qin, H.; Rivero, I.V. Mechanical behavior of bimetallic stainless steel and gray cast iron repairs via directed energy deposition additive manufacturing. *J. Manuf. Process.* **2023**, *85*, 1197–1207. [\[CrossRef\]](#)
- Xu, Q.; Li, M.; Yang, L.; Su, B.; Liu, X.; Zou, D.; Shi, T.; Yue, X. Grain refinement and associated strengthening in laser additive repaired uranium. *J. Nucl. Mater.* **2024**, *593*, 154995. [\[CrossRef\]](#)
- Chu, M.; Xiao, H.; Ren, L.; Mo, T.; Lin, B. Microstructure and properties of Ti–Al–C composite coatings prepared by laser cladding. *Ceram. Int.* **2024**, *50*, 12498–12509. [\[CrossRef\]](#)
- Jie, Z.; Qunli, Z.; Jianhua, Y.; Zhisheng, W.; Li, K. Process Optimization and Interfacial Microstructure and Properties Analysis of Laser Cladded IN718 Alloy. *Chin. J. Lasers Zhongguo Jiguang* **2022**, *49*, 1602021.
- Jiahui, C.; Jiahao, W.; Song, Z.; Lei, W.; Li, H. Impact of Ultrasonic Surface Rolling Processes on Microstructures and Fatigue Properties of 300M Steel Laser-Cladding-Repaired Components. *J. Mater. Eng. Perform.* **2024**, 1–11. [\[CrossRef\]](#)
- Chen, W.; Chen, H.; Li, C.; Wang, X.; Cai, Q. Microstructure and fatigue crack growth of EA4T steel in laser cladding remanufacturing. *Eng. Fail. Anal.* **2017**, *79*, 120–129. [\[CrossRef\]](#)
- Chen, L.; Chen, W.; Huang, Q. Effect of ultrasonic vibration on quality and properties of laser EA4T steel. *J. Mater. Eng.* **2019**, *47*, 79–85.
- Du, Y.; Peng, Y.; Liang, Q.; Li, Z.; Tu, J. Effect of heat treatment on microstructure and mechanical properties of Fe60 coating by laser cladding on 304 stainless steel. *J. Mater. Res. Technol.* **2024**, *29*, 2825–2834. [\[CrossRef\]](#)
- Ma, M.; Nie, S.; Yu, H.; Huang, G.; Wang, X.; Zhang, N. Effect of Heat Treatment on Microstructure and Wear Behavior of Laser Clad FeCoCrMoNi High-Entropy Alloy Coatings. *J. Mater. Eng. Perform.* **2024**, 1–11. [\[CrossRef\]](#)
- Wang, S.; Wang, L.; Li, J.; Li, T.; Qiu, Y.; Yang, R. Effect of heat treatments on mechanical properties and wear resistance of laser-powder bed-fused Ti6Al4V alloy. *Mod. Phys. Lett. B* **2024**, *38*, 2450245. [\[CrossRef\]](#)
- Shan, L.; Ji, T.; Jinghui, L.; Qiang, Z.; Jing, C. Effect of Solution Aging Heat Treatment on Microstructure Evolution and Properties of TC17 Titanium Alloy Formed by Laser Solid Forming. *J. Mater. Eng. Perform.* **2023**, *33*, 2002–2014.
- Li, F.; Qi, B.; Zhang, Y.; Guo, W.; Peng, P.; Zhang, H.; He, G.; Zhu, D.; Yan, J. Effects of Heat Treatments on Microstructures and Mechanical Properties of Ti6Al4V Alloy Produced by Laser Solid Forming. *Metals* **2021**, *11*, 346. [\[CrossRef\]](#)
- Jianbo, L.; Xiaohui, L.; Jing, B.; Tong, Z.; Yunhua, X.; Yuan, Y. Effects of Thermal Treatment on Microstructure and Wear Properties of Ni60/CeO₂ Composite Coating 35CrMoV Steel by Laser Cladding. *Coatings* **2022**, *12*, 1575. [\[CrossRef\]](#)
- Ge, M.; He, Z.; Wang, L.; Fu, H.; Wu, W.; Chen, Z.; Cheng, H.; Si, T.; Che, L.; Zheng, K.; et al. The influence of annealing temperature on the microstructure and mechanical properties of Fe-0.52 C-11Mn-5.14Al-1Cr lightweight steel. *Mater. Today Commun.* **2024**, *40*, 109464. [\[CrossRef\]](#)
- Liu, Z.; Xu, G.; Zhang, Y.; Zhang, L.; Huang, J. Influence of multiple short-time normalizations on mechanical properties and microstructure of 9Cr-2.3W-3.0Co heat-resistant steels. *Mater. Sci. Eng. A* **2023**, *879*, 145282. [\[CrossRef\]](#)
- Chen, B.; Zhang, G.; Zhang, Z.; Wang, Z.; Guo, C.; Song, X. Improved wear and corrosion resistance of laser-clad (Fe_{0.25}Co_{0.25}Ni_{0.25}Cr_{0.125}Mo_{0.125})₈₆B₁₄ coating through annealing treatment. *Surf. Coat. Technol.* **2023**, *473*, 129973. [\[CrossRef\]](#)
- Dong, H.; Guo, P.-F.; Han, Y.; Bai, R.-X.; Yang, Z.-C.; Zhang, S.-Q. Enhanced corrosion resistance of high speed laser-cladded Ni/316L alloy coating by heat treatment. *J. Mater. Res. Technol.* **2023**, *24*, 952–962. [\[CrossRef\]](#)
- Shi, S.; Huang, C.; Liu, F.; Chen, W.; Liu, F.; Xia, C. Effect of heat treatment on microstructure and mechanical properties of 34CrNiMo6 steel by laser solid forming. *J. Manuf. Process.* **2022**, *78*, 308–318. [\[CrossRef\]](#)
- Fang, Z.; Tieming, G.; Qiang, L.; Yan, Y.; Ruihua, Z.; Xueli, N. Effect of solution aging treatment on microstructure and properties of Fe-0.5C-11Cr corrosion resistant alloy by laser cladding. *J. Alloys Compd.* **2022**, *78*, 308–318.
- Zhang, Y.; Bai, P.; Li, Z.; Zhang, J.; Liu, W. Multi-objective optimization of laser cladding process parameters for Q345B steel. *Mater. Today Commun.* **2024**, *39*, 108679. [\[CrossRef\]](#)
- Zhang, J.; Zhu, H.; Qiu, C.; Shen, L. Influence of scanning strategies on laser-cladded AISI 420 steel. *Surf. Eng.* **2022**, *38*, 948–956. [\[CrossRef\]](#)

24. GB/T 4340.1-2009; Vickers Hardness Test Method for Metallic Materials. National standard of the People's Republic of China: Beijing, China, 2009.
25. GB/T 229-2007; Charpy Pendulum Impact Test Method for Metallic Materials. National standard of the People's Republic of China: Beijing, China, 2007.
26. Changyao, O.; Rui, W.; Chunjiang, Z.; Runze, W.; Huan, L.; Rui, D.; Qiaofeng, B.; Yingliang, L. Study on ductile iron surface laser cladding austenitic stainless steel coating heat treatment to enhance wear resistance. *Tribol. Int.* **2023**, *191*, 109202.
27. Liu, H.; Liu, J.; Li, X.; Chen, P.; Yang, H.; Hao, J. Effect of heat treatment on phase stability and wear behavior of laser clad AlCoCrFeNiTi_{0.8} high-entropy alloy coatings. *Surf. Coat. Technol.* **2020**, *392*, 125758. [[CrossRef](#)]
28. Gao, Z.; Zhang, S.; Gao, Z.; Ren, H.; Zhang, C. Effect of Heat Treatment on Microstructure and Tribological Properties of Laser Cladding CeO₂/Ni60 Composite Coating on 35CrMoV Steel. *Coatings* **2023**, *13*, 161. [[CrossRef](#)]
29. Chen, C.; Wang, J.; Ge, Y.; Zhuang, M.; Ma, Z. Microstructure and Wear Resistance of High-Chromium Cast Iron with Multicomponent Carbide Coating via Laser Cladding. *Coatings* **2023**, *13*, 1474. [[CrossRef](#)]
30. Wennan, S.; Chi, Z.; Xiufang, C.; Guo, J.; Changhao, L.; Erbao, L.; Jian, L.; Haonan, Z.; Boyu, C.; Haoliang, T. Effect of heat and cryogenic treatments on the microstructure and properties of YF₃ modified NiTi-Si laser cladding coatings. *Opt. Laser Technol.* **2023**, *165*, 109614.

Disclaimer/Publisher's Note: The statements, opinions and data contained in all publications are solely those of the individual author(s) and contributor(s) and not of MDPI and/or the editor(s). MDPI and/or the editor(s) disclaim responsibility for any injury to people or property resulting from any ideas, methods, instructions or products referred to in the content.